Transactions on Machine Intelligence 3(1) (2020) 43–56

ISSN Online: 2821-1693

Transactions on Machine Intelligence

Journal Homepage: https://tmachineintelligence.ir/index.php/TMI

Modeling the Human Sinoatrial Node Based on Sequential Discharge Hypothesis

R. Yaghoobi Karimi[1], S. Azadi[1,*], O. Rahamni Seryasat[2]

[1] Department of Biomedical Engineering, Semnan University, Semnan, Iran
[2] Department of Electrical Engineering, Faculty of Technology and Engineering, Shams Higher Education institute, Gorgan, Iran.

ARTICLE INFO

Article History:
Received 22 December 2019
Received in revised form
15 February 2020
Accepted 25 March 2020
Available online 26 March 2020

Keywords:
Large Mammalian; Human;
Sinoatrial Node Model;
Modified Hodgkin-Huxley Model;
Pacemaker Activity.

ABSTRACT

Achieving electrical synchronization among sinoatrial (SA) node cells, which is essential for initiating and propagating pacemaker activity, remains a complex and widely discussed issue in cardiac electrophysiology. While several previous studies have proposed theoretical models to explain this synchronization, the majority have been limited to small-scale simulations involving only a few interconnected SA node cells. To address this limitation, the present study introduces a novel computational model of the human SA node grounded in the sequential discharge hypothesis. This model features a three-dimensional (3D) lattice of cells governed by a modified Hodgkin-Huxley (HH) framework, where the membrane dynamics are adjusted using a time constant to simulate realistic propagation of action potentials through gap junctions. Simulation results demonstrate that the proposed model can produce stable oscillatory activity within a physiological heart rate range of 40 to 180 beats per minute (BPM). Furthermore, the 3D network effectively estimates the extracellular electrical potential in the vicinity of the SA node, closely matching the signals recorded by clinical electrodes. These findings suggest that the model offers a more comprehensive and scalable approach for studying the electrical synchronization mechanisms of large populations of SA node cells, particularly in human cardiac tissue.

1. INTRODUCTION

The SA node is a group of coupled nerve cells positioned on the wall of the right atrium, near the entrance of the superior vena cava [1]. This ellipsoid node has volume about 15 millimeters long 3 millimeters, wide and 1 millimeter thick [2]. The electrical activity of this node is the primary origin of a very important biological signal called electrocardiogram (ECG) [3] that controls the heart rate by using the nervous impulses of autonomic nervous

* Corresponding Author: azadieng@yahoo.com, sazadi@semnan.ac.ir
Associate professor, Department of Biomedical Engineering, Semnan University, Semnan, Iran

http://dx.doi.org/10.47176/TMI.2020.43

system [4-5]. Hence, the nerve cells of SA node can generate the electrical impulses in a specific frequency range. This frequency range in different mammalian depends on body size [6], so that the heart rate of small mammalian is more than that of large mammalian. The presence of this difference, especially in the resting heart rate, causes that many researchers have provided different mathematical models such as the Bristow-Clark model [7], the Irisawa-Noma model [8] and the Noble-Noble model [9-10], Wilders model [11] and Lovell model [12] for the SA node cells of small mammalian like rabbit.

Some of researchers by increasing the membrane capacitance and by adding new ion channels [13] expressed that these models are functionally suitable for modeling the human SA node cells, while they cannot fundamentally generate oscillations in the range of the human heart rate (50 (sleep) to 120 (exercise) beats per minute) [24]. Because, these models are a derivation of the Hodgkin-Huxley (HH) model, which its oscillation frequency is more than several BPM [14]. Hence, increasing the membrane capacitance in these models not only increases the width of action potential, but also reduces the amplitude of action potentials (Fig. 1). On the other hand, since two ion channels: sodium and potassium in the HH model play a fundamental role in determining the oscillation rate, Adding new ion channels to the HH models usually decreases the period of action potentials [11]. However, these channels can modify the shape of action potential. Therefore, the width of action potentials generated by these models not only is not compatible with the action potentials of a single SA node cell (Fig. 1), but also the period of action potentials in modified models is less than the HH model. In the other word, the outputs of these models are suitable for the spikes generated by a group of SA node cells in small mammalian such as rat and rabbit.

The SA node includes a aggregation of coupled nerve cells that each of these cells has volume about 5 micrometer wide and 80 micrometer long and 5 micrometer thick [15]. Many gap junctions join the membrane of these nerve cells to each other, so that the ion flow without action potentials can travel from one cell to the next, and create a delayed action potential in next cells [16]. These asynchronous activities in the cells generate the electrical spikes around the SA node that electrodes measure them. Therefore, we in this work provide a new model for the SA node that consists of a three-dimensional regular network of coupled cells. The remainder of this paper is organized as follows: Section 2 presents two of effective factors in the HH model. Section 3 and 4 proposes a modified HH model for generating the pacemaker activity in the range 40 to 180 BPM. Section 5 models the SA node based on the sequential discharge hypothesis. Finally, section 6 presents the discussion and conclusion.

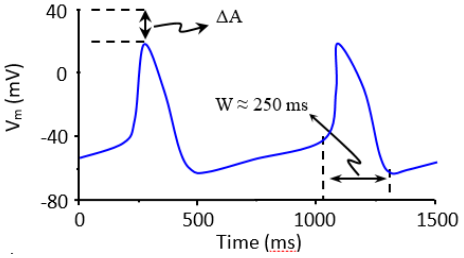

Fig. 1. Pacemaker activity of human SA node reported by Verkerk, et al., 2009 [13]

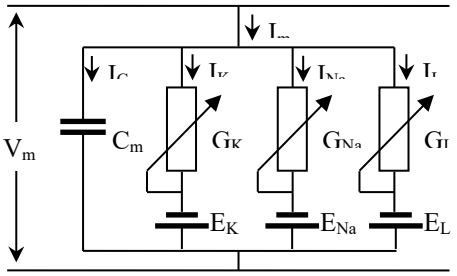

Fig. 2. The equivalent circuit of Hodgkin-Huxley model

2. HODGKIN-HUXLEY MODEL

Hodgkin-Huxley model is a parallel conductance model that approximates the electrical characteristics of excitable cells such as neurons [17]. Fig. 2 illustrates the equivalent circuit of Hodgkin-Huxley model. This model consists of three components of ionic conductance: fast-sodium, delay-potassium and leakage (other ions). These three components were obtained by using the voltage clamp experiments of squid axon [18].

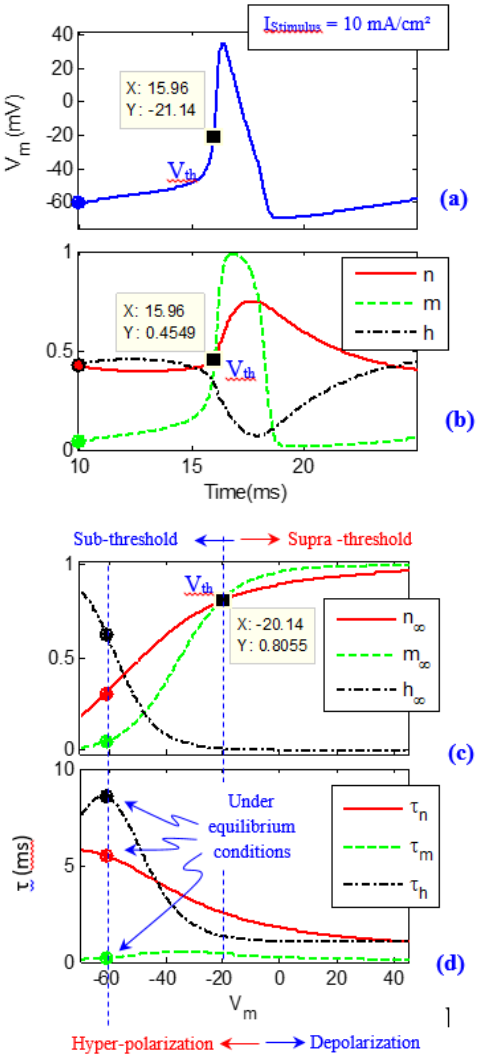

Fig. 3. The action potential created under a constat stimulus current 10 mA/cm^2, and the variation of x, x_∞ and τ_x to V_m for the Hodgkin-Huxley model

3.1. Threshold voltage

The Hodgkin-Huxley for modeling the delay-potassium and fast-sodium conductance at voltage clamp defined three probabilistic parameters (particles) n, m, h and the transfer rate of particles (α and β). They generally decided to formulate the changes of these three parameters at voltage clamp as follows [18]:

$$x(t) = x_\infty - (x_\infty - x_0)e^{-t/\tau_x} \quad x = \{n, m, h\} \tag{1}$$

Then, they modeled the x_∞ and τ_x by using the transfer rates α_x and β_x, which were extracted from the voltage clamp experiments of squid axon. Fig. 3a depicts the action potentials created under a constant stimulus current 10

mA/cm^2. The changes of parameters x, x_∞ and τ_x for the Hodgkin-Huxley model are shown in figures 3b to 3d. As shown in Fig. 3c, the crossing point of two curves n and m is equivalent with threshold voltage, so that if value n crosses from this point ($m > n$), the HH model generates an action potential. Therefore, the period of action potentials generated by the HH model is determined by the time to reach to this point.

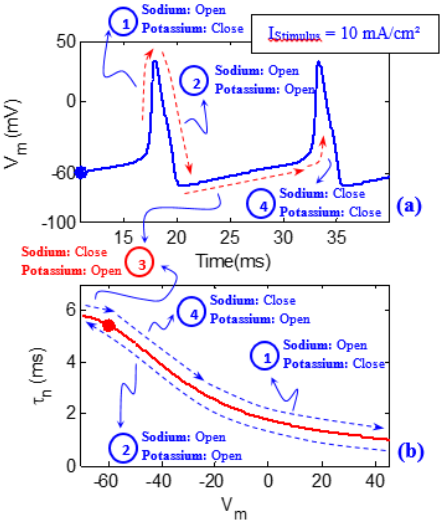

Fig. 4. a) The analysis of action potential generated by the HH model, b) Relationship of τ_n to V_m

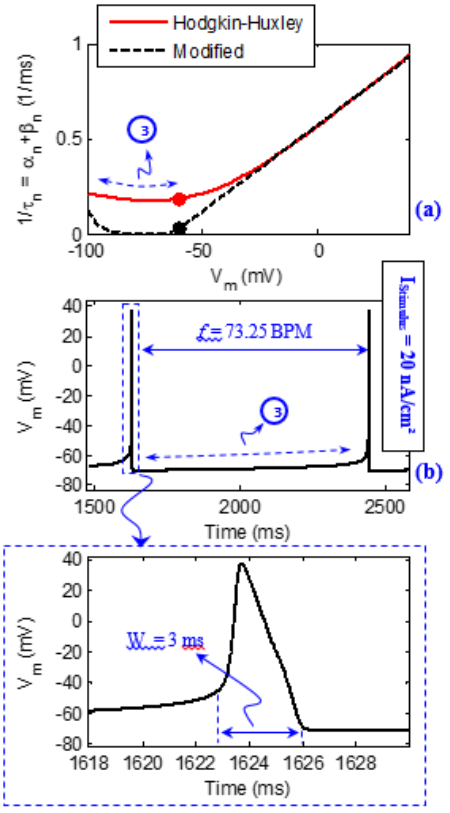

Fig. 5. a) Relationship of $1/\tau_n$ to V_m, b) the action potential of modified model under a constant stimulus current 10 mA/cm^2

3.2. Effect τ_n on the oscillation frequency

We have shown that the period of action potentials in the HH model depend on the time to reach to the threshold voltage. Therefore, we focus more on Fig. 3 for increasing this time. As shown in this figure, the value of parameter τ_n in the neighborhood of equilibrium point plays an important role for changing the period of action potentials. Therefore, we can divide an action potential into four sections (Fig. 4), which third section is relevant to the charging time of membrane voltage after an action potential. In the other word, increasing the τ_n in this section can increase the period of action potentials. Hence, we increase the period of action potentials by just changing this section of τ_n. In the following section, we explain our modification.

3. MODIFIED MODEL FOR A SINGLE SA NODE CELL

We varied the equation τ_n of Hodgkin-Huxley model as following:

$$\tau_n = \frac{1 - e^{-(V_m+63)}}{0.009(V_m+63) + 0.125\left(1 - e^{-(V_m+63)}\right)e^{-\frac{V_m+100}{5}}} \tag{2}$$

This equation increases the time constant of τ_n around its equilibrium point, especially in the membrane voltages -70 to -60 mV. Fig. 5a shows curve $1/\tau_n$ for two models. As seen in figure, the $1/\tau_n$ of the modified model in the neighbourhood of equilibrium point is less than that of the HH model. Therefore, this model has more time to reach the resting and threshold voltage. On the other hand, since this equation dose not creates the change in other section (1, 2 and 4 in Fig. 4b) of τ_n, the shape (width and amplitude) of action potentials generated by this model are almost equal to the HH model. In the subsection next, we add two new ion channels for generating the spontaneous discharge in the modified model and also replace an inward background current with the constant stimulus current ($I_{Stimulus}$) and the leakage channel for changing the firing rate of modified model.

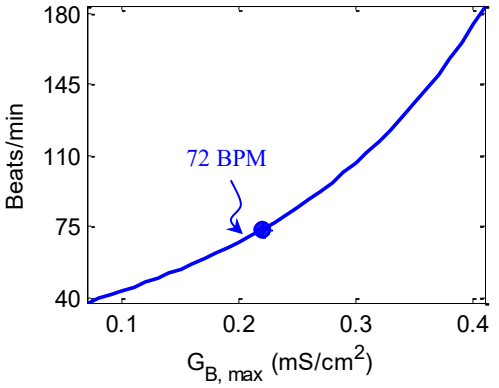

Fig. 6. Plot of repetitive firing frequency vs. $G_{B,\,max}$

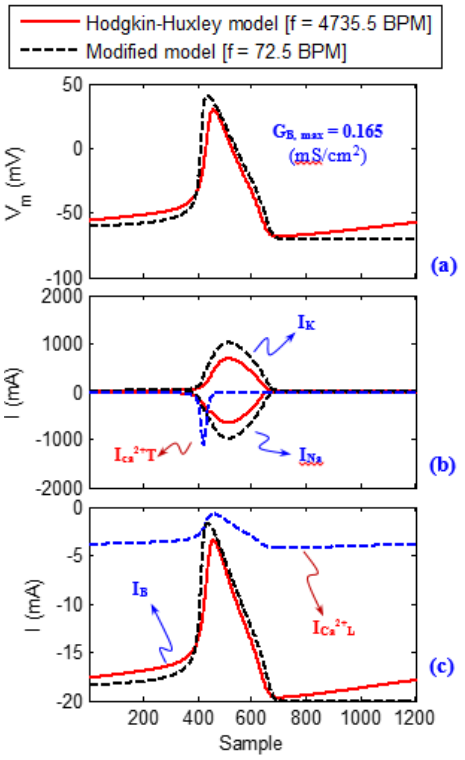

Fig. 7. a) Membrane voltage, b) The currents of fast-sodium, delay-potassium and transient (T) calcium, c) The currents of long-lasting (L) calcium and inward background

4. SPONTANEOUS DISCHARGE

Although, recent physiological evidences indicate that the membrane voltage, inward background current and calcium channels jointly regulate the spontaneous discharge of SA node [11], each of these factors has a specific role in the spontaneous discharge of SA node cells. Accordingly, we added two calcium channels: transient (T) and long-lasting (L) type to our model for creating pacemaker activity. In addition, we define an inward background current obtain from the resultant of background ionic exchanges for changing the oscillation frequency of our model. In fact, this current component is an alternative to the constant stimulus current that it is used to charge the membrane voltage after repolarization. Appendix A provides the equation of our model for a single SA node cell. We defined the inward background current as following.

$$I_B = G_{B,\max}\left(V_m - E_B\right) \tag{3}$$

Where $G_{B,\max}$ and E_B are the maximum value of background conductance and a positive Goldman voltage for ions, respectively. Fig. 6 shows the effect of $G_{B,\max}$ on the number of action potentials generated in one minute. As shown in this figure, the modified model can generate oscillations between 40 and 180 BPM, while $G_{B,\max}$ just changed between 0.07 and 0.41. Therefore, this model not only can be an alternative model for each of the human SA node cells, but also parameter $G_{B,\max}$ can be a control point for the autonomic nervous system. On the other hand, comparing the shape of membrane voltage and the current of ion channels in both models (Fig. 7) show that the modified model does not creates the change in the shape of model outputs ($G_{B,\max} = 0.165\ mS/cm^2$). In the subsection next, we used this model to provide a new SA node base on sequential discharge hypothesis

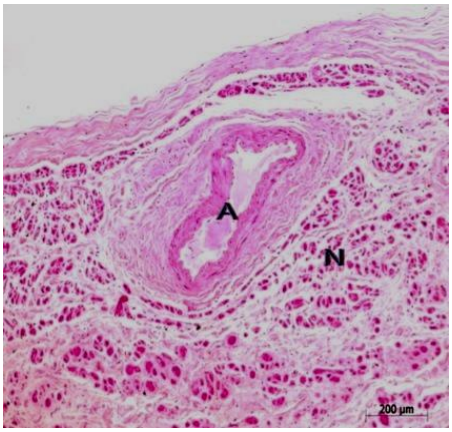

Fig. 8. Histological image of the SA node: A) indicates the SA nodal artery, N) indicates the SA nodal cells [19].

5. MODELING THE SA NODE BASE ON SEQUENTIAL DISCHARGE HYPOTHESIS

5.1. Model structure

Aggregation of cells in the SA node (Fig. 8) caused that researchers have proposed different hypotheses [20] for the electrical synchronization of SA node cells. Since, each of SA node cells intrinsically oscillates in a certain frequency. Also, since each of these cells excites the cells of a particular part of the heart. One of provided hypotheses is the sequential discharge of SA node cells synchronized by a dominant pacemaker for generating a set of delayed action potentials.

According to this hypothesis, a dominant pacemaker, which is a cell or small group of cells in the SA node, creates the sequential discharge by driving other SA node cells. Hence, we in this research used a three-dimensional regular network to establish the mentioned hypothesis. Fig. 9 indicates this three-dimensional regular network.

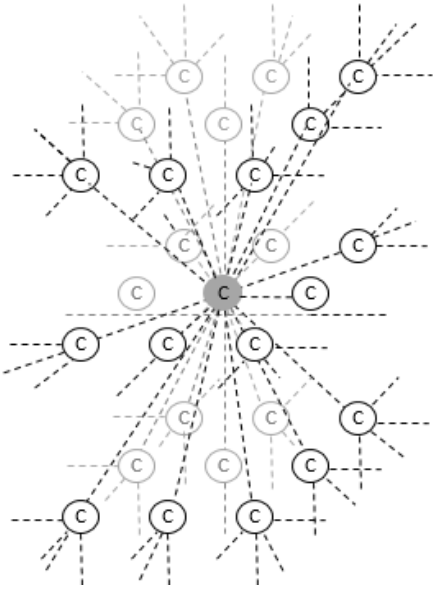

Fig. 9. Three-dimensional regular network considered for the SA node. This figure only shows two first layer of network, which includes cells and gap junction.

We modeled all of the network cells by using the modified HH model (section 3), with the exception that only the cell (or small group of cells) of first layer (C_1) had the spontaneous discharge. Also, we used the voltage-dependent conductance of gap junctions (g_j) reported by Spray, et al., 1981 [21] for coupling the SA node cells and modeled the g_j according to Bennett- Verselis model Bennett and Verselis, 1992 [22] as following.

$$g_j = \frac{\left(g_{j,\max} - g_{j,\min}\right)^2}{\left(1+e^{\frac{V_m+E_j}{A}}\right)\left(1+e^{-\frac{V_m+E_j}{A}}\right)} + g_{j,\min} \tag{4}$$

Where E_j is the voltage at which $p_0 = pc$. A is a constant expressing gating charge. $g_{j,\min}$ and $g_{j,\min}$ are minimum and maximum value of g_j.

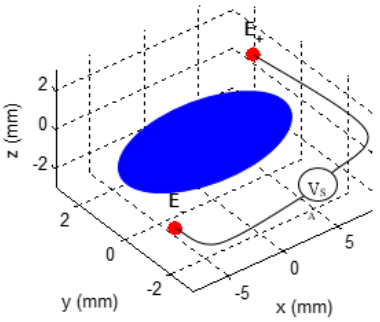

Fig. 10. Schematic of SA node used in the study with volume about 45 mm^3

5.2. Electrical potential around the model

As shown in Fig. 9, each of the network cells excites a group of next layer cells through gap junctions. Since, each of cells works as supra –threshold and the gap junctions transfer the ion flow as sub-threshold, we considered each of cells as an electrical dipole, which it consists of two monopoles of opposite sign but equal strength q_{ij} separated by the gap junction. Therefore, the electrical potential for the *j*th dipole of *i*th layer at t time is calculated as follows [18,23].

$$V_{ij}(t) = \frac{q_{ij}(t) d \cos\theta_{ij}}{4\pi\varepsilon\varepsilon_0 r_{ij}^2} \qquad d_{ij} << r_{ij} \tag{5}$$

Where d_{ij} is the displacement from negative to positive point charge. r_{ij} is distance dipole from a certain point around the electrical dipole. θ_{ij} is angle between vector r_{ij} and the bipolar axes. $q_{ij}(t)$ is intercellular or extracellular ion exchange in the *j*th cell of *i*th layer at t time that is equivalent with charge accumulated on each of the capacitor plate in the modified HH model. Therefore, we can rewrite the $q_{ij}(t)$ as following.

$$q_{ij}(t) = C_{ij} V_{ij,m}(t) \tag{6}$$

Where C_{ij} and $V_{ij,m}(t)$ are the membrane capacitance and voltage in the *j*th cell of *i*th layer at t time, respectively.

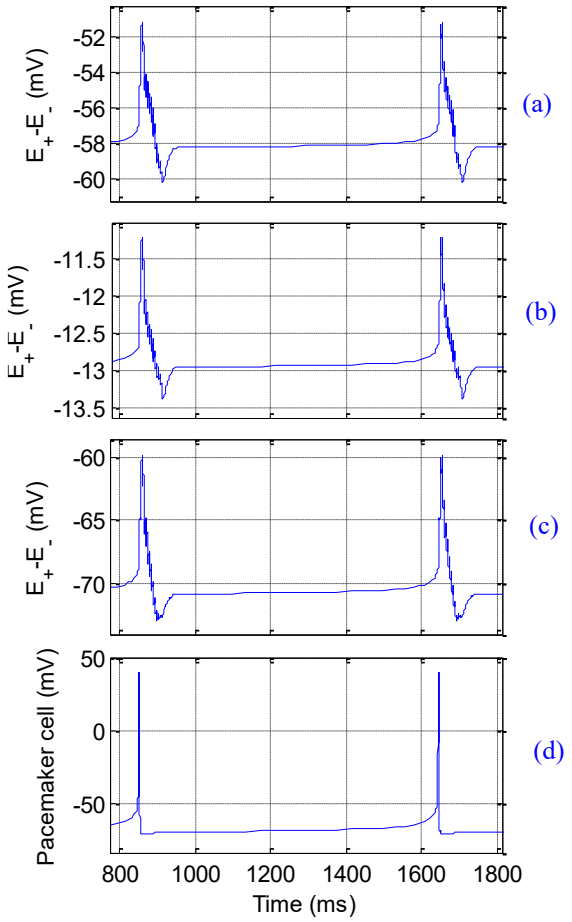

Fig. 11. The potential difference of two electrodes in positions: a) E+ (5,0,5) & E- (-5,0,-5), b) E+ (10,0,10) & E- (-10,0,-10), c) E+ (3,3,3) & E- (-3,-3,-3) d) The membrane potential of pacemaker cell

We assumed that the cells are circular with diameter about 90 micrometers. Since, the SA node has volume about 45 mm^3 (3 millimeters wide, 15 millimeters long and 1 millimeter thick), the three-dimensional regular network for this volume was included 42 layers and 4010 cells. Therefore, the electrical potential of a point around the network according to the principle of superposition is equivalent with the sum of electrical potential of these cells. Fig. 10 schematically indicates the SA node that it consists of a three-dimensional regular network of SA node cells with 42 layers. We computed the potential difference of two electrodes located in E_+ and E_- (V_{SA}).

Fig. 11 shows the membrane potential of pacemaker cell and the potential difference of two electrodes in three different positions. Although, the activity amplitude of these potential differences is less than that of action potential of a SA node cell, their activity time is more (Fig. 11d). Because, this potential difference is a resultant of all SA node cells (the three-dimensional regular network). On the other hand, as seen in Fig. 11a-c, the shape of the potential difference depends on the position of two electrodes. Fig. 11a and Fig. 11b shows the effect of distance from the SA node and Fig. 11c shows the effect of position change in the electrodes.

Fig. 12 represents the activity of three-dimensional regular network (SA node) at time 857.9 ms. As seen in this figure, each of the network layers at this time has a different activity level. In fact, these activity levels (discharges) are generated in the pacemaker cell and are propagated through the gap junctions to next layers. The propagation of these discharges according to the principle of superposition creates an electrical potential around the SA node, which we usually record these electrical potential by electrodes.

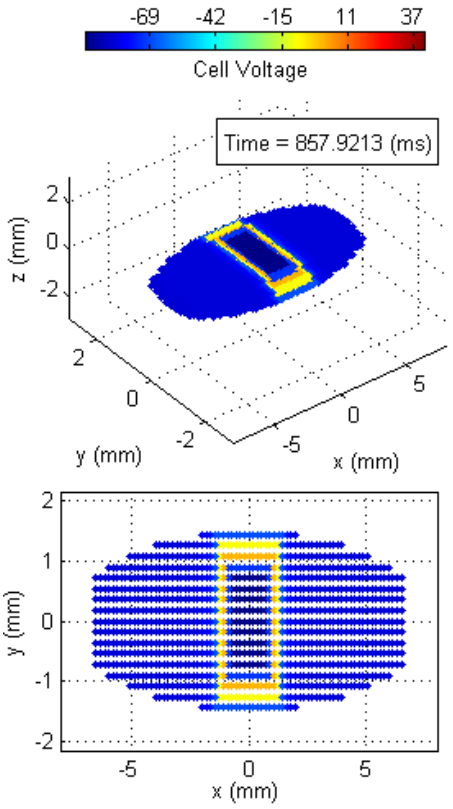

Fig. 12. The activity of three-dimensional regular network (SA node) at time 857.9 ms: a) 3D view, b) x-y view

6. DISCUSSION AND CONCLUSION

Although, the mammalian SA node cells have a similar pacemaker activity, the firing rate of these cells in various mammalians depends on their body size. Therefore, the modified HH models due to the different dynamic of these cells in small mammalians cannot generate the firing rate proportional to large mammalians such as human. On the other hand, increasing the membrane capacitance of HH model cannot create a firing rate 50 to 180 BPM without increasing the width of action potentials. So, a new factor is demanding to generate such a firing rate in the HH model.

The analysis of Hodgkin-Huxley model in this study has shown that increasing the value of section 3 in the τ_n increases the time to reach to the threshold voltage after the hyper-polarization. Therefore, this section of τ_n is a fundamental factor for increasing the firing rate of HH model, so that defining a new equation for the τ_n can simply tune the HH model to oscillate in the range of 50 to 180 BPM without increasing the width of action potentials. Also, this analysis indicates that we can generate and change the spontaneous discharge by adding three ion channels: transient (T) calcium channel, long-lasting (L) calcium channel and inward background current (Fig. 6).

Another of challenges of the SA node is relationship of the electrical potential around the SA node to the action potentials of SA node cells. Since, these cells unlike electronic circuits, that use the electrical field for the transmission of waves, use a propagation phenomenon for the transmission of action potential. Also, since the gap junctions propagate the ion flow without action potentials from one cell to the next, we based on sequential discharge hypothesis can consider the SA node as an aggregation of electrical dipoles with time-variant charges. As shown in the results of this research, the electrical potential around SA node according to the principle of superposition is equivalent with the sum of electrical potential of these dipoles. Therefore, this approach not only can be very useful to study the dynamic of SA node, but also it can be suitable to model the electrical activity of different sections of

heart in future. However, some experimental verification is needed to validate the modified Hodgkin-Huxley and SA node models provided in this study.

Appendix A: The equation of modified HH model

- *Trans-membrane current*

$$\begin{aligned} C_m \frac{dV_m}{dt} = &-G_{Na}(V_m - E_{Na}) - G_K(V_m - E_K) \\ &- G_{Ca^{2+}L}(V_m - E_{Ca^{+2}L}) - G_{Ca^{2+}T}(V_m - E_{Ca^{+2}T}) \\ &- G_{B,max}(V_m - E_B) \end{aligned} \tag{6}$$

- *Ionic conductances*

$$\frac{dx}{dt} = \frac{x_\infty - x}{\tau_x} \tag{7}$$

$$x = \{n, m, h, d_L, f_L, f_{Ca^{2+}}, d_T, f_T\}$$

$$G_K = G_{K,max} n^4 \tag{8}$$

$$G_{Na} = G_{Na,max} m^3 h \tag{9}$$

$$G_{Ca^{2+}T} = G_{Ca^{2+}T,max} d_T f_T \tag{10}$$

$$G_{Ca^{2+}L} = G_{Ca^{2+}L,max} d_L f_L f_{Ca^{2+}} \tag{11}$$

- *Transfer rate coefficients*

$$\tau_n = \frac{1 - e^{-(V_m+63)}}{0.009(V_m + 63) + 0.125\left(1 - e^{-(V_m+63)}\right)e^{-\frac{V_m+100}{5}}} \tag{12}$$

$$\tau_m = \frac{\left(1 - e^{-\frac{Vm+35}{10}}\right)}{0.1(Vm+35) + 4\left(1 - e^{-\frac{Vm+35}{10}}\right)e^{-\frac{Vm+60}{20}}} \tag{13}$$

$$\tau_h = \frac{\left(1 + e^{-\frac{Vm+30}{10}}\right)}{1 + 0.07\left(1 + e^{-\frac{Vm+30}{10}}\right)e^{-\frac{Vm+60}{20}}} \tag{15}$$

$$\tau_{d_L} = \frac{1}{\alpha_{d_L} + \beta_{d_L}} \tag{16}$$

$$\alpha_{d_L} = \frac{-0.02839(Vm+35)}{e^{-\frac{Vm+35}{2.5}} - 1} - \frac{-0.0849Vm}{e^{-\frac{Vm}{4.8}} - 1}$$

$$\beta_{d_L} = \frac{0.01143(\mathrm{Vm}-5)}{e^{\frac{\mathrm{Vm}-5}{2.5}}-1}$$

$$\tau_{f_L} = 257.1e^{-\left(\frac{\mathrm{Vm}+35.5}{13.9}\right)^2} + 44.3 \quad (17)$$

$$\tau_{fCa^{2+}} = \frac{f_{Ca^{2+},\infty}}{\alpha_{f_{Ca^{2+}}}} \quad (18)$$

$$\tau_{d_T} = \frac{1}{1.068e^{\frac{\mathrm{Vm}+26.3}{30}} + 1.068e^{-\frac{\mathrm{Vm}+26.3}{30}}} \quad (19)$$

$$\tau_{f_T} = \frac{1}{0.0153e^{-\frac{\mathrm{Vm}+61.7}{83.3}} + 0.015e^{\frac{\mathrm{Vm}+61.7}{15.38}}} \quad (20)$$

$$n_\infty = \frac{(\mathrm{Vm}+50)}{12.5\left(1-e^{-\frac{\mathrm{Vm}+50}{10}}\right)e^{-\frac{\mathrm{Vm}+60}{80}} + (\mathrm{Vm}+50)} \quad (21)$$

$$m_\infty = \frac{0.1(\mathrm{Vm}+35)}{0.1(\mathrm{Vm}+35) + 4\left(1-e^{-\frac{\mathrm{Vm}+35}{10}}\right)e^{-\frac{\mathrm{Vm}+60}{20}}} \quad (22)$$

$$h_\infty = \frac{0.07\left(1+e^{-\frac{\mathrm{Vm}+30}{10}}\right)}{e^{\frac{\mathrm{Vm}+60}{20}} + 0.07\left(1+e^{-\frac{\mathrm{Vm}+30}{10}}\right)} \quad (23)$$

$$d_{L,\infty} = \frac{1}{1+e^{-\frac{\mathrm{Vm}+14.1}{6}}} \quad (24)$$

$$f_{L,\infty} = \frac{1}{1+e^{-\frac{\mathrm{Vm}+30}{5}}} \quad (25)$$

$$f_{Ca^{2+},\infty} = \frac{\mathrm{K}_{\mathrm{mfCa}^{2+}}}{\mathrm{K}_{\mathrm{mfCa}^{2+}} + [Ca^{2+}]_{sub}} \quad (26)$$

$$d_{T,\infty} = \frac{1}{1+e^{-\frac{\mathrm{Vm}+26.3}{6}}} \quad (27)$$

$$f_{T,\infty} = \frac{1}{1+e^{\frac{\mathrm{Vm}+61.7}{5.6}}} \quad (28)$$

- *Constants*

Constants	Value	Unit	Ref
V_r	-60	mV	[1]
Ej	0	mV	-
E_{Na}	55	mV	[1]
E_K	-72	mV	[1]
E_L	49.387	mV	[1]
$E_{Ca^{2+}L}$	45	mV	[2]
$E_{Ca^{2+}T}$	45	mV	[2]
C_m	5	μF/cm^2	-
$G_{Na,\,max}$	120	mS/cm^2	[1]
$G_{K,\,max}$	36	mS/cm^2	[1]
$G_{L,\,max}$	0.3	mS/cm^2	[1]
$G_{Ca^{2+}L,\,max}$	120	mS/cm^2	-
$G_{Ca^{2+}T,\,max}$	50	mS/cm^2	-
$K_{mfCa^{2+}}$	0.00035	mM	[2]
$[Ca2+]_{sub}$	20	mM	-
$\alpha_{fCa^{2+}}$	0.035	1/cm^2	[2]
$G_{j,min}$	0.01	mS/cm^2	-
$G_{j,max}$	10	mS/cm^2	-
A	20	mV	-
d	90	nm	-
ε_0	8.854e-12	F/m	[1]
ε	2	-	-

Note: [1] Malmivuo and Plonsey, 1995 , [2] Kurata, et al., 2002

- *equilibrium conditions*

Constants	Value	Unit
V_{m0}	- 60.39	mV
$n_{,0}$	0.7976	-
m_0	0.2138	-
h_0	0.1092	-
d_{L0}	0.4466	-
f_{L0}	0.9526	-
$f_{Ca^{2+}0}$	4.99e-4	-
d_{T0}	0.1015	-
f_{T0}	0.0040	-

CONFLICTS OF INTEREST

The authors declare no conflict of interest.

REFERENCES

[1] Campbell, N. A., & Reece, J. B. (2009). Biology: Concepts & Connections. Pearson/Benjamin Cummings.
[2] Guyton, A. C., & Hall, J. E. (2006). Textbook of Medical Physiology. Elsevier Saunders.
[3] Israel, S. A., Irvine, J. M., Cheng, A., Wiederhold, M. D., & Wiederhold, B. K. (2005). ECG to identify individuals. Pattern Recognition, 38, 133–142. https://doi.org/10.1016/j.patcog.2004.05.014
[4] Byrne, D. G., & Rosenman, R. H. (1990). Anxiety and the heart. International College of Psychosomatic Medicine.
[5] Robertson, D. (2014). Primer on the autonomic nervous system (2nd ed.; I. Biaggioni, G. Burnstock, P. A. Low, D. Robertson, & J. Paton, Eds.). Academic Press.
[6] Dawson, T. H. (2014). Allometric relations and scaling laws for the cardiovascular system of mammals.

Systems, 2(2), 168–185. https://doi.org/10.3390/systems2020168
[7] Bristow, D. G., & Clark, J. W. (1982). A mathematical model of primary pacemaking cell in SA node of the heart. American Journal of Physiology - Heart and Circulatory Physiology, 243(2), H207–H218. https://doi.org/10.1152/ajpheart.1982.243.2.H207
[8] Irisawa, H., & Noma, A. (1982). Pacemaker mechanisms of rabbit sinoatrial node cells. In Cardiac Rate and Rhythm (pp. 35–51). https://doi.org/10.1007/978-94-009-7535-4_4
[9] Noble, D., Difrancesco, D., & Denyer, J. C. (1989). Ionic mechanisms in normal and abnormal cardiac pacemaker activity. In Neuronal and Cellular Oscillators (pp. 59–85).
[10] Noble, D., & Noble, S. J. (1984). A model of sino-atrial node electrical activity based on a modification of the DiFrancesco–Noble (1984) equations. Proceedings of the Royal Society of London. B: Biological Sciences, 222(1228), 295–304. https://doi.org/10.1098/rspb.1984.0065
[11] Wilders, R., Jongsma, H. J., & Van Ginneken, A. C. (1991). Pacemaker activity of the rabbit sinoatrial node: A comparison of mathematical models. Biophysical Journal, 60(5), 1202–1216. https://doi.org/10.1016/S0006-3495(91)82155-5
[12] Lovell, N. H., Cloherty, S. L., Celler, B. G., & Dokos, S. (2004). A gradient model of cardiac pacemaker myocytes. Progress in Biophysics and Molecular Biology, 85(2–3), 301–323. https://doi.org/10.1016/j.pbiomolbio.2003.12.001
[13] Verkerk, A. O., van Ginneken, A. C. G., & Wilders, R. (2009). Pacemaker activity of the human sinoatrial node: Role of the hyperpolarization-activated current, If. International Journal of Cardiology, 132(3), 318–336. https://doi.org/10.1016/j.ijcard.2008.12.196
[14] Connor, J. A., Walter, D., & McKown, R. (1977). Neural repetitive firing: Modifications of the Hodgkin-Huxley axon suggested by experimental results from crustacean axons. Biophysical Journal, 18(1), 81–102. https://doi.org/10.1016/S0006-3495(77)85598-7
[15] Verkerk, A. O., Wilders, R., Van Borren, M. M. G. J., Peters, R. J. G., Broekhuis, E., Lam, K., … Tan, H. L. (2007). Pacemaker current (If) in the human sinoatrial node. European Heart Journal. https://doi.org/10.1093/eurheartj/ehm339
[16] Verheule, S., van Kempen, M. J. A., Postma, S., Rook, M. B., & Jongsma, H. J. (2001). Gap junctions in the rabbit sinoatrial node. American Journal of Physiology. Heart and Circulatory Physiology, 280(5), H2103–H2115. https://doi.org/10.1152/ajpheart.2001.280.5.H2103
[17] Cronin, J. (1987). Mathematical Aspects of Hodgkin-Huxley Neural Theory. Cambridge University Press. https://doi.org/10.1017/CBO9780511983955
[18] Malmivuo, J., & Plonsey, R. (1995). Bioelectromagnetism: Principles and Applications of Bioelectric and Biomagnetic Fields. Oxford University Press. https://doi.org/10.1093/acprof:oso/9780195058239.001.0001
[19] Tohno, Y., Tohno, S., Viwatpinyo, K., Minami, T., Chaisuksunt, V., Mahakkanukrauh, P., & Quiggins, R. (2014). Age-related changes of elements in the human sinoatrial nodes. OA Anatomy, 2, 1–6.
[20] Michaels, D. C., Matyas, E. P., & Jalife, J. (1987). Mechanisms of sinoatrial pacemaker synchronization: A new hypothesis. Circulation Research, 61(5), 704–714. https://doi.org/10.1161/01.RES.61.5.704
[21] Spray, D. C., Harris, A. L., & Bennett, M. V. (1981). Equilibrium properties of a voltage-dependent junctional conductance. The Journal of General Physiology, 77(1), 77–93. https://doi.org/10.1085/jgp.77.1.77
[22] Bennett, M. V. L., & Verselis, V. K. (1992). Biophysics of gap junctions. Seminars in Cell Biology, 3(1), 29–47. https://doi.org/10.1016/S1043-4682(10)80006-6
[23] Cheng, D. K. (1989). Field and Wave Electromagnetics. Addison-Wesley.
[24] Fuster, V., O'Rourke, R. A., Walsh, R., & Poole-Wilson, P. (2007). Hurst's The Heart (12th ed.). McGraw-Hill Education.
[25] Kurata, Y., Hisatome, I., Imanishi, S., & Shibamoto, T. (2002). Dynamical description of sinoatrial node pacemaking: Improved mathematical model for primary pacemaker cell. American Journal of Physiology. Heart and Circulatory Physiology, 283(5), H2074–H2101. https://doi.org/10.1152/ajpheart.00900.2001